International Journal of Biological Macromolecules 279 (2024) 135173

Contents lists available at ScienceDirect

International Journal of Biological Macromolecules

journal homepage: www.elsevier.com/locate/ijbiomac

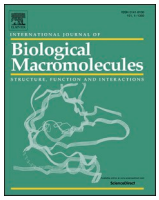

Development and characterization of polylactic acid/starch biocomposites – From melt blending to preliminary life cycle assessment

Hossein Baniasadi [a,*,1], Laura Äkräs [a,1], Zahra Madani [b], Frans Silvenius [c], Mahyar Fazeli [d], Sami Lipponen [a], Jaana Vapaavuori [b], Jukka Seppälä [a]

[a] Polymer Technology, School of Chemical Engineering, Aalto University, Kemistintie 1, 02150 Espoo, Finland
[b] Department of Chemistry and Materials Science, Aalto University, Kemistintie 1, 02150 Espoo, Finland
[c] Bieconomy and Environment, Natural Resources Institute Finland, Latokartanonkaari 9, 00790 Helsinki, Finland
[d] Department of Bioproducts and Biosystems, School of Chemical Engineering, Aalto University, FI-00076 Aalto, Finland

ARTICLE INFO

Keywords:
Polylactic acid
Starch
Biocomposite
Life cycle assessment
3D printing

ABSTRACT

This study presents a comprehensive analysis encompassing melt blending, characterization, life cycle assessment (LCA), and 3D printing of a range of polylactic acid (PLA)/starch biocomposites, with starch content varying from 0 to 50 wt%. To enhance compatibility between the starch particles and the PLA matrix, we utilized a solvent-free method to graft N-octadecyl isocyanate (ODI) molecules onto the surface of the starch particles, resulting in ODI-*g*-starch, which yielded several improved properties. Notably, toughness and elongation at break improved by approximately 170 % and 300 %, respectively. Moreover, the crystallinity increased from 11.6 % in plain PLA to 30.1 %, suggesting that the uniform dispersion of ODI-*g*-starch particles acted as nucleating sites for the crystallization of PLA chains. Additionally, viscosity decreased significantly with the introduction of ODI-*g*-starch particles, indicating their plasticizing effect, thereby enhancing the processability and ease of fabrication of the biocomposite. Crucially, our LCA analysis revealed a significant reduction in the carbon footprint of these biocomposites, up to 18 % and 63 %, compared to plain PLA and selected fossil-based plastics, respectively, upon the incorporation of ODI-*g*-starch. In summary, our research introduces the newly developed PLA/starch biocomposites as a sustainable and eco-friendly alternative to commercially available plain PLA and specific fossil-based plastics.

1. Introduction

In today's world, global concerns emerge large, with pressing issues such as climate change, environmental pollution, and the diminishing reserves of crude oil resources. These challenges are primarily driven by the excessive and often uncontrolled use of fossil-based and non-biodegradable plastics, prompting a shift away from commonly used petroleum-based polymers. Simultaneously, this global awareness has spurred interest in exploring sustainable and biodegradable alternatives that can meet our daily life needs [1–4]. In this context, biodegradable polymers like poly(butylene succinate) (PBS), poly(3-hydroxybutyrate) (PHB), thermoplastic starch (PTA), and polylactic acid (PLA) have emerged as practical solutions to mitigate plastic waste [5–7].

PLA, in particular, stands out as a versatile alternative to traditional synthetic polymers like polypropylene (PP), polyethylene (PE), and polystyrene (PS). It boasts excellent tensile strength, high stiffness, and favorable physical properties [8–10]. Additionally, PLA is commonly used in food and beverage packaging [5,6], and it possesses a low carbon footprint [11,12]. Its environmental performance can also be further enhanced through blending with various biofillers [13–16]. Nonetheless, PLA, like most bioplastics, is often more expensive than its fossil-based counterparts and comes with certain technical limitations, including excessive brittleness, limited flexibility, challenging processing characteristics, inferior barrier properties, and low melt strength [17]. Blending PLA with naturally occurring polymers, such as cellulose and starch, offers a potentially cost-effective solution without compromising biodegradability [5,6,18].

Starch, in particular, is a highly promising biopolymer due to its wide availability, versatility, renewability, cost-effectiveness, and suitability for industrial applications. Notably, starch exhibits excellent oxygen

* Corresponding author.
E-mail address: hossein.baniasadi@aalto.fi (H. Baniasadi).
[1] H.B. and L.Ä. contributed equally to this work.

https://doi.org/10.1016/j.ijbiomac.2024.135173
Received 10 April 2024; Received in revised form 29 May 2024; Accepted 27 August 2024
Available online 28 August 2024

barrier properties, making it an attractive candidate for food packaging, especially for preserving fruits [9,19,20]. In this context, PLA/starch blends have garnered significant attention as promising biodegradable composites, especially in food packaging [21–24]. Under specific conditions, these blends can completely biodegrade into carbon dioxide (CO_2) and water [4]. Nevertheless, because PLA is hydrophobic while starch is hydrophilic, direct blending often results in thermodynamically immiscible blends with poor interfacial adhesion, low strength, high brittleness, and reduced toughness, rendering them unsuitable for practical applications [22,25]. To address these challenges, various strategies have been explored to enhance the compatibility of starch and PLA. One well-studied approach involves incorporating suitable plasticizers, such as glycerol, ethylene glycol, xylitol, propylene glycol, and diethylene glycol, into the blending process. Another extensively researched strategy revolves around surface-treating starch through grafting copolymers like poly(ε-caprolactone) and polyethylene glycol, as well as chemically crosslinking it with maleic anhydride, acrylic acid, and glycidyl methacrylate [9,25,26].

Life cycle assessment (LCA), on the other hand, is crucial when developing a new composite material as it evaluates the environmental impacts throughout the product's life cycle, from raw material extraction to disposal. By providing a holistic view of energy consumption, emissions, and resource use, LCA helps to identify areas for improvement, ensuring that sustainability goals are met without shifting environmental burdens. It supports informed decision-making, regulatory compliance, and market acceptance by demonstrating a commitment to reducing the ecological footprint. Ultimately, LCA guides the development of composites that are environmentally friendly, economically viable, and socially responsible [27–29].

Consequently, it has recently been used to investigate the environmental impacts of PLA and PLA composites. For instance, Mai et al. [30] modified cellulose nanofiber surfaces with diisocyanate compounds to create hydrophobic isocyanate-modified fibers, enhancing their compatibility with PLA. They evaluated various properties of the developed composites, including impacts through LCA, to demonstrate the feasibility of quantifying the environmental impacts of producing PLA composites. Their assessment revealed that incorporating modified cellulose nanofiber had a small impact on the environmental effects compared to corn grain-based PLA, except for the impact categories of global warming and fossil resource scarcity. Furthermore, a comparative analysis performed by Torsello et al. [31] revealed that integrating carbon dots not only enhanced the performance of the PLA membranes but also underscored the commitment to sustainable and environmentally conscious material design. Additionally, a preliminary LCA conducted on the PLA/thermoplastic starch composites confirmed that it is possible to obtain materials with properties similar to polypropylene, with carbon footprint reductions of 33.6 % [2]. Further, a cradle-to-gate LCA study on green composites made of PLA filled with different amounts of natural lignocellulosic fibers, obtained from pine needles or kenaf fibers, concluded that the green composites were substantially less impactful than pure PLA. The environmental benefits increased with the higher filler content, resulting in up to 48 % reduction in greenhouse gas (GHG) emissions and 32 % reduction in primary energy demand, respectively, for the composites containing 40 % of fibers [15].

Considering this framework, this study focused on the development of a series of PLA/starch biocomposites. The objective was to create materials that combine excellent technical performance with environmental friendliness, contrasting them with plain PLA and fossil-based plastics as reference materials. Our approach involved surface-treating potato starch through a urethane reaction between the hydroxyl groups of starch and n-octadecyl isocyanate molecules. Subsequently, different concentrations of surface-treated starch were melt-blended to produce the biocomposites. Furthermore, we conducted a preliminary cradle-to-gate LCA of the newly developed PLA/starch biocomposite granules to evaluate their carbon footprint and identify early-stage development hotspots. Finally, serving as a practical demonstration of the applications for the newly developed, eco-friendly biocomposites, filaments of consistent diameter were extruded, using the biocomposite with 50 wt% starch, and employed in 3D printing to create a complex prototype with precise dimensions and high surface quality.

2. Experimental and methodological setup

2.1. Materials

Polylactic acid (PLA), with a molecular weight of 175,000 g/mol, was sourced from Corbion Biochem in the Netherlands. Furthermore, we procured potato starch, n-octadecyl isocyanate (ODI, technical grade), and synthetic indigo (with a dye content of 95 %) from Sigma-Aldrich. Ethanol (Etax B) was purchased from Anora Industrial in Finland.

2.2. Compatibilization

A solvent-free method was established to graft the ODI on the surface of starch to enable compatibility between these starch particles and the PLA matrix [33–35]. Initially, 100 g of starch was thoroughly vacuum-dried at 70 °C for 24 h. Subsequently, the dried starch and 20 g of ODI were placed in a preheated oven set at 110 °C. This system remained in the oven for 8 h at 110 °C to facilitate the urethane reaction between the hydroxyl groups of starch and the cyanate groups of ODI, resulting in the formation of a substance referred to as ODI-*g*-starch. Finally, these surface-treated starch particles underwent two ethanol washes to eliminate any unreacted ODI, followed by an overnight drying of ODI-*g*-starch at room temperature. For a visual representation of the reaction between ODI molecules and starch particles, refer to Fig. S1.

2.3. Melt blending and injection molding

The PLA granules were subjected to thorough vacuum drying at 50 °C for 24 h. Subsequently, they were physically mixed with varying concentrations of ODI-*g*-starch (10, 20, 30, 40, and 50 wt%, respectively). The resulting mixture was introduced into a counter-rotating twin-screw extruder (DSM, The Netherlands) that had been preheated to 200 °C. Next, the components were melt-blended at 20 rpm, cooled on a conveyor equipped with a cooling fan, and then granulated using a pelletizer.

The biocomposite granules were later fed into an injection molding machine to produce specimens for tensile and impact testing. However, prior to injection molding, both plain PLA and the pelletized PLA/starch blends were dried in a Conair Churchill dryer for 2 h at 55 °C to minimize PLA hydrolysis during the melt processing. Following drying, the materials were immediately injection molded into test specimens (ISO 527, specimen type 1 A) using an Engel ES 200/40 injection molding machine. A gentle dosing procedure was employed to prevent excessive PLA degradation: the four heating zones were set at 155 °C (Feed), 180 °C, 180 °C, and 180 °C (Die), with a dosing speed of 30 % and a counter pressure set to 1 bar. Additionally, during the injection step, an injection speed of 100 mm/s was used, with a mold temperature of 15 °C, followed by an after-pressure step of 45 bar for 20 s (for plain PLA and biocomposites containing <30 wt% of starch). For biocomposites containing 40 and 50 wt% of starch, the applied after-pressure was reduced to 20 and 10 bar, respectively. Besides, hot-pressed biocomposite films were prepared using a lab press (Fontijne Lab Press-TP 400, The Netherlands) at 200 °C. Table 1 provides an overview of the sample names and their respective compositions.

2.4. Characterization

2.4.1. Analysis of the functional groups

Fourier-transform infrared (FTIR) spectroscopy was conducted using an ATR spectrometer integrated with an FTIR instrument (PerkinElmer, USA) to analyze the functional groups present in starch before and after

Table 1
Overview of sample names and compositions.

Sample name	PLA composition (%)	ODI-*g*-starch composition (%)
PLA	100	0
P90S10	90	10
P80S20	80	20
P70S30	70	30
P60S40	60	40
P50S50	50	50

the surface treatment. The spectra were recorded at room temperature, covering a wavenumber range from 4000 cm^{-1} to 500 cm^{-1}, with 16 scans and a resolution of 4 cm^{-1}.

2.4.2. Elemental analysis

To assess the extent of ODI grafting, the levels of carbon (C), hydrogen (H), nitrogen (N), sulfur (S), and oxygen (O) in both native starch and starch after the surface treatment were quantified using a CHNSO elemental analyzer (Thermo Flash Smart, USA). To establish a reference point, theoretical values of C, O, and H elements in native starch (calculated based on the anhydroglucose formula $C_6H_{10}O_5$) were compared with the measured elemental quantities. This information was used to construct a standard curve, with measured values plotted against the theoretical ones (refer to Fig. S2). Subsequently, the elemental measurements for ODI-*g*-starch were adjusted using the calibration curve to determine the percentage of grafted ODI molecules according to Eq. (1).

$$DS = \frac{72.07 - C \times 162.14}{295.5 \times C - 228.20} \quad (1)$$

Here, C represents the calibrated carbon element concentration in ODI-*g*-starch. The values 72.07 and 162.14 correspond to the carbon mass in the starch glucose unit and the molecular weight of the glucose unit, respectively. Additionally, 295.5 and 228.20 denote the molecular weight and carbon mass in the ODI molecule. Each measurement was conducted in triplicate, and the reported values represent the mean of these measurements, accompanied by the standard deviation.

2.4.3. Analysis of microstructure

The morphology of starch particles before and after surface treatment, as well as the microstructure of the fracture surfaces in the biocomposites, were investigated using scanning electron microscopy (SEM) with a Zeiss Sigma VP instrument from Germany. To prepare the samples, the biocomposites were fractured under the influence of liquid nitrogen and coated with a thin layer (~ 4 nm) of gold palladium. The same sputtering process was also applied to starch and ODI-*g*-starch particles. SEM imaging was conducted using a voltage of 2 kV.

2.4.4. Study of crystallinity

The crystallization behavior of plain PLA, biocomposites, starch, and ODI-*g*-starch was examined using a differential scanning calorimeter (DSC) – specifically, the TA Instruments Discovery DSC 250 Auto – under a nitrogen atmosphere. The tests were conducted over a temperature range of 0 to 200 °C, with a scanning rate of 10 °C/min. Two heating-cooling cycles were performed within the same temperature range and rate. All samples were maintained isothermally for 5 min at boundary temperatures, specifically 0 and 200 °C.

To calculate crystallinity (χc), Eq. (2) was utilized, where ΔH_m and ΔH_{cc} represent the melting and cold crystallization enthalpies, respectively [36]. The variable 'x' denotes the weight percentage of ODI-*g*-starch in the blends, while ΔH_m^0 corresponds to the melting enthalpy of 100 % crystalline PLA, which is 93.6 J/g [37].

$$\chi(\%) = \frac{\Delta H_m - \Delta H_{cc}}{(1 - x)\Delta H_m^0} \times 100 \quad (2)$$

2.4.5. Analysis of thermal decomposition

Thermogravimetric analysis (TGA) was performed using a TA Instruments TGA Q500 instrument (USA), operating under a nitrogen flow rate of 25 mL/min, over a temperature range from 30 to 800 °C. The thermograms served a dual purpose: firstly, to assess the percentage of grafted ODI molecules on starch particles, and secondly, to monitor the thermal decomposition behavior of both PLA and the biocomposites.

2.4.6. Mechanical properties

Tensile testing was conducted using a Universal Tester Instron (4204, USA) in accordance with ASTM D638–02 standards. The testing parameters included a load cell of 5 kN and a tensile rate of 5 mm/min. Prior to testing, the samples were conditioned at a temperature of 24 °C and a relative humidity of 55 % for 72 h. Typical stress-strain curves were utilized to derive the following mechanical properties: tensile modulus (MPa), yield stress (MPa), tensile strain or elongation at break (%), and toughness (J/m^3). For the impact test, specimens of ISO 191-1 type 1 (without a notch) were tested according to ASTM standards on a Charpy ZwickRoell machine. Five measurements were conducted, and the reported result represents the mean value along with the standard deviation.

2.4.7. Dynamic mechanical analysis

The viscoelastic behavior of both plain PLA and the biocomposites, encompassing parameters such as tan δ, storage modulus (E'), and loss modulus (E"), was investigated over a temperature range of 30 to 110 °C using a dynamic mechanical analyzer (DMA Q800, TA Instruments, USA). Consistent test conditions were maintained across all samples, including a strain amplitude of 1 %, a frequency of 1 Hz, a pre-load of 1 N, and a heating rate of 3 °C/min. The glass transition temperature (T_g) was determined by identifying the peak in the tan δ curves.

2.4.8. Rheology analysis

Dynamic rheological testing was conducted using a rotational rheometer, specifically the Anton Paar Physica MCR 301 from Austria. To establish the linear viscoelastic region, a strain sweep test was initially performed at a fixed angular frequency of 10 rad/s, covering a shear strain range from 0.01 % to 100 %. Subsequently, a dynamic frequency sweep test was conducted under a constant strain amplitude of 1 %, spanning a frequency range from 0.1 to 600 rad/s. All measurements were carried out at a temperature of 200 °C, employing PP25/Al and PP50/Al geometries.

2.5. Preliminary life cycle assessment

2.5.1. Goal and scope definition

The objective of preliminary LCA was to quantify the carbon footprint and identify the key environmental impact areas, the hotspots, in the laboratory-scale production of novel PLA/starch biocomposite granules, with varying the proportion of potato starch as the biofiller from 10 wt% to 50 wt%. The ultimate aim of this study was to establish an initial understanding of the carbon footprint associated with the newly developed biocomposites, with the potential for this data to inform future material and process enhancements. To accomplish these objectives, the present LCA was conducted in accordance with the ISO 14040 and 14044 standards [38,39]. The study's system boundaries, further, encompassed the life cycle from the cultivation of bio-based feedstock to the production of biocomposite granules. This comprehensive scope, therefore, included the sourcing and processing of essential raw materials, such as potato starch, ODI, and PLA granules, as well as the manufacturing of PLA/starch biocomposite granules under laboratory conditions. For a simplified visual summary of the system boundaries, please refer to Fig. 1.

Additionally, the preparation of specimens and filaments for the PLA/starch biocomposites, as well as their End-of-Life (EoL)

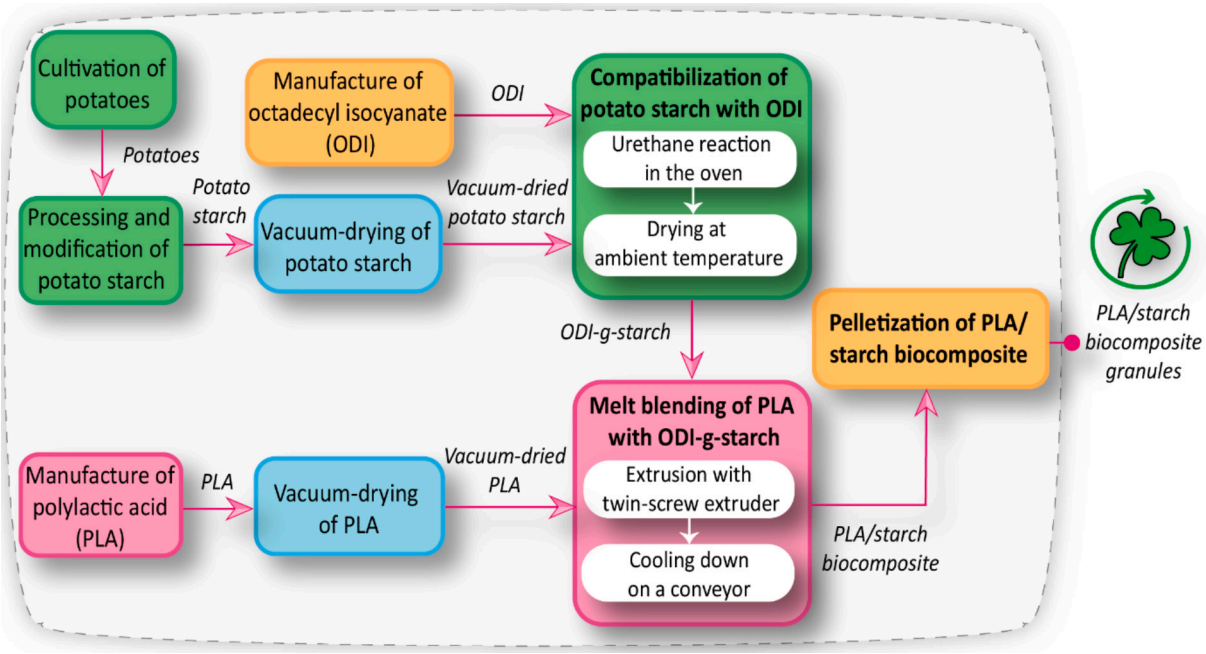

Fig. 1. System boundaries for the PLA/starch biocomposite granules from cradle to gate. In this figure, the dashed line delineates the system boundaries, while the colored blocks represent the individual unit processes examined in this study. The material transportation is not depicted in this scheme.

considerations, were intentionally omitted from the analysis. As for the functional unit, it was defined as 1 kg of biocomposite granules. The regional context for the analysis, in turn, included the following regions: Finland (for potatoes, potato starch, and PLA/starch biocomposite granules), France (for ODI), and Thailand and the Netherlands (for PLA granules), respectively.

2.5.2. Life cycle inventory (LCI)

The LCI data in this study incorporates primary, secondary, and tertiary sources. Specifically, the data related to potatoes was gathered from a confidential case study conducted by the Natural Resources Institute Finland. Similarly, information on potato starch was obtained from the confidential case study by the Natural Resources Institute Finland as well as from the databases, such as Ecoinvent v3.8 (published in 2021) and Sphera Solutions GmbH's Sphera Managed LCA Content (MLC) 2023.2. LCI data for ODI was exclusively sourced from the MLC databases. Conversely, the data concerning the production of PLA/starch biocomposite granules primarily originated from the laboratory-scale experiments. For other parameters, we either supplemented the data with information available in the MLC databases or calculated them by using Eq. S1 and Table S1, which detail the calculations and electricity values for various laboratory equipment, respectively. The collected LCI data for the primary laboratory processes involved in manufacturing the PLA/starch biocomposite granules is tabulated in Tables S2–S6. However, we have not included data from the Natural Resources Institute Finland and Ecoinvent/MLC databases in this paper due to their confidential and commercial nature, respectively.

Furthermore, LCI data for transporting potato starch, ODI, and PLA from their manufacturers to Aalto University was obtained from the MLC databases and supplemented with data collected from the scientific literature [40], especially regarding the types of vehicles and fuel used. On the other hand, the distances covered during transportation were estimated using Google Maps [41], Fluent Cargo [42], and other relevant sources. The selection of departure and arrival points was, further, guided by Google Maps [41], Fluent Cargo [42], SeaRates [43], and additional literature sources [44–49], as well as datasets in LCA for Experts (LCA FE) and the experimental section of this paper. Detailed transportation information for potato starch, ODI, and PLA is comprehensively outlined in Table S7.

2.5.3. Data and modeling assumptions

The dataset employed in the LCA FE software, representing a mixture of aliphatic isocyanates, was chosen as a substitute for ODI due to the limited availability of precise data for this particular material. Furthermore, ethanol was omitted from the analysis because it was solely used to wash unreacted ODI after the compatibilization step, and it did not play a role in the production of the biocomposite granules.

In terms of assumptions, the duration of use for the vacuum oven and oven during the vacuum-drying of potato starch/PLA and the compatibilization of PLA and ODI-g-starch, respectively, were based on the actual heating times of the equipment. Moreover, the power consumption of laboratory equipment was estimated either from the actual measurements, from equipment or manufacturer websites, or through reasonable assumptions. The moisture content of PLA before vacuum-drying was assumed to be 4 %. Additionally, no losses of substances resulting from the laboratory experiments, even in small quantities, were considered in the present LCA.

Regarding the processes in LCA FE, tap water, sourced from groundwater, and municipal wastewater treatment, coupled with agricultural sludge application in the processing and modification of potato starch, was substituted with European processes due to the unavailability of Finnish equivalents. For the processing and modification of potato starch, Ecoinvent data was obtained from the United States, Europe in general, Germany, and Finland. Furthermore, in the case of land transport of PLA granules in Thailand, the process involving Indian diesel mix was used as a proxy due to the absence of a Thai alternative.

2.5.4. Sensitivity analysis

In the current study, we applied sensitivity analysis to assess the uncertainty related to the computed electricity values for various laboratory equipment, given the relatively significant impact of electricity within the defined system boundaries. To examine this further, we conducted the analysis by substituting the baseline case, which employed Finnish electricity, with two alternative scenarios known as sensitivity analysis scenarios 1 and 2. These scenarios involved the use of European (EU-28) and global green electricity, respectively.

2.5.5. Life cycle impact assessment (LCIA)

The current LCA was conducted by using Sphera Solutions GmbH's Software LCA FE along with the MLC databases 2023.2 [50]. The chosen impact category for the assessment was carbon footprint, expressed as kilograms of CO_2 equivalent per kilogram of biocomposite granules. In this study, we also took into account the sequestration of CO_2 in the potato starch, and its calculation was based on Eq. (3) [95].

$$CDR(CO_2) = \left(\frac{\left(\frac{M(C)_{ST}}{M(ST)}\right) \cdot m(ST)_{biocompositegranules}}{\left(\frac{M(C)_{CO2}}{M(CO_2)}\right)} \right) \cdot Cf(CO_2) \quad (3)$$

where $CDR(CO_2)$ stands for the amount of sequestered CO_2 in potato starch, $M(C)_{ST}$ for the molecular weight of carbon in potato starch, M (ST) for the molecular weight of potato starch, $m(ST)_{biocomposite\ granules}$ for the amount of potato starch required for 1 kg of PLA/starch biocomposite granules, $M(C)_{CO2}$ for the molecular weight of carbon in CO_2, $M(CO_2)$ for the molecular weight of CO_2, and $Cf(CO_2)$ for the characterization factor of CO_2.

2.6. Filament preparation and 3D printing

The filaments for fused deposition modeling (FDM) 3D printing were produced using the same extruder as the compounding process, with the only difference being that the blending temperature was set at 190 °C. Achieving the appropriate filament diameter, precisely 2.70 ± 0.25 mm, was accomplished through trial and error by carefully controlling the screw and conveyor speeds. Additionally, a small amount of indigo dye was incorporated into the PLA/ODI-*g*-starch blend before the blending process to introduce colour to the granules/filaments. For the 3D printing process, a Lulzbot-mini desktop FDM printer from the USA was employed. The specific priming conditions are detailed in Table S8.

3. Results and discussion

3.1. Surface treatment of starch

The grafting of ODI molecules onto the surface of starch particles was thoroughly investigated using multiple analytical techniques, including FTIR spectra, TGA thermograms, elemental analysis results, and SEM images. Fig. 2a illustrates the FTIR spectra, which effectively captures the transformation of starch before and after the surface treatment. In the initial state, the native starch exhibited distinct characteristic bands, including an O—H stretching band at 3285 cm^{-1}, C—H stretching from alkyl groups at 2930 cm^{-1}, H_2O bending vibration at 1642 cm^{-1}, C—H bending at 1450 cm^{-1}, C—O stretching at 1244 cm^{-1}, C-OH stretching at 1200 cm^{-1}, C—O stretching of -C-O-H at 1152 cm^{-1}, C-O-H stretching at 1100 cm^{-1}, C—O bond stretching of -C-O-C at 1085 cm^{-1}, and CH2 bending at 991 cm^{-1} [26,51].

Following the modification process, these aforementioned peaks were still discernible in the ODI-*g*-starch spectrum. Notably, the intensity of several peaks underwent significant alterations, and novel characteristic bands emerged, signifying the successful grafting of ODI molecules onto the starch surface. For instance, the characteristic peak at 3300 cm^{-1}, corresponding to hydroxyl groups, exhibited a substantial reduction in intensity, suggesting their involvement in an urethane reaction with the cyanate groups of ODI. Furthermore, two distinct bands emerged at approximately 2920 cm^{-1} and 2855 cm^{-1}, which were attributed to the antisymmetric and symmetric stretching of C—H bonds in the alkyl long chain of ODI [52]. Additionally, two peaks at 1613 cm^{-1} and 1572 cm^{-1} became apparent, corresponding to amide I and amide II vibrations, respectively. Notably, the absence of the isocyanate (-N=C=O) characteristic band at 2273 cm^{-1} confirmed that any unreacted ODI molecules were effectively removed during the washing process with ethanol and acetone [53].

The quantification of grafted ODI molecules onto starch particles was carefully tracked through TGA/DTG analysis and elemental analysis. Fig. 2b showcases the TGA/DTG thermograms, highlighting the transformations in starch before and after surface modification. Initially, the native starch exhibited two distinct weight loss regions. The first, occurring at around 100 °C, resulted in a 9.2 % reduction in mass, attributed to the evaporation of starch moisture. The second, observed at 300 °C, entailed a substantial 77 % weight loss, associated with the pyrolytic decomposition phase of starch (comprising amylose and amylopectin) [54,55].

Notable deviations were observed in the TGA/DTG thermograms of starch following ODI grafting. Specifically, the initial weight loss due to moisture evaporation became significantly milder, with a mass decrease of approximately 2.6 %, indicating that ODI-*g*-starch exhibited markedly lower hydrophilicity than unmodified starch. Additionally, a new decomposition step emerged at approximately 270 °C, with a weight loss of 12 %, corresponding to the decomposition of ODI molecules, akin to the decomposition observed in the case of plasticizer molecules in plasticized starch [56]. In essence, TGA/DTG thermograms indicated an approximately 12 % grafting of ODI molecules onto the starch particles.

Furthermore, the weight residue of the surface-treated starch at 800 °C (16.3 %) exceeded that of untreated starch (13.85 %), likely attributed to the char residue from ODI molecules [57]. It's worth noting that, in some studies, an increased dispersity in the starch decomposition peak has been reported, indicating disruptions in the crystalline configuration and non-uniform thermal stability of starch after surface treatment, potentially leading to reduced thermal stability [58,59]. However, in this current study, the dispersity of the starch decomposition peak remained unaltered after surface treatment, suggesting minimal impact from the applied modification method on the thermal stability of starch.

The elemental analysis results, summarized in Table 2, were instrumental in providing a more precise estimation of the quantity of grafted ODI molecules. Substantial disparities in the levels of carbon (C), oxygen

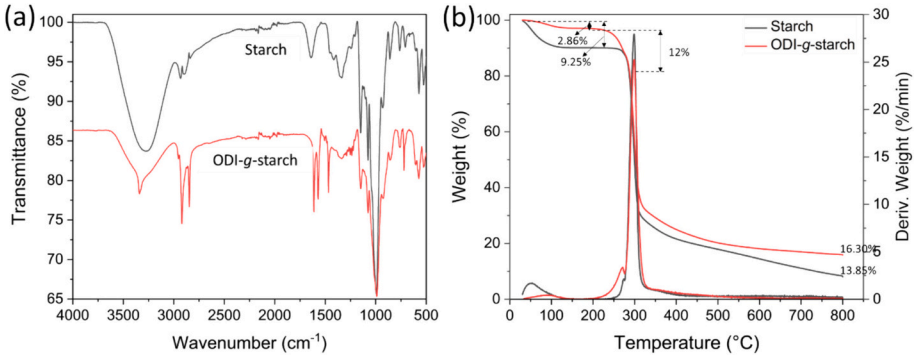

Fig. 2. a) FTIR spectra and b) TGA/DTG thermograms of the plain and surface-treated starch.

Table 2
The elemental analysis results.

Sample	Carbon (%)	Hydrogen (%)	Nitrogen (%)	Oxygen (%)	Sulfur (%)	DS[a]	ODI (wt%)
Starch[b]	44.64	6.19	0	49.16	0	–	–
Measured values							
Starch	37.50 ± 0.06	6.09 ± 0.10	0	50.26 ± 0.19	0	–	–
ODI-*g*-starch	45.18 ± 0.52	6.94 ± 0.09	0.37 ± 0.05	47.87 ± 0.12	0	–	–
Corrected values							
Starch	39.90	6.70	0	52.23	0	–	–
ODI-*g*-starch[c]	48.03	7.59	0.64	50.87	0	0.067	12.27

[a] Calculated from Eq. (1).
[b] Theoretical values regarding the anhydroglucose formula, $C_6H_{10}O_5$.
[c] Regarding the calibration curve (Fig. S2).

(O), hydrogen (H), and nitrogen (N) elements were observed between starch before and after surface treatment. Notably, while the native starch exhibited no nitrogen content, the ODI-*g*-starch displayed approximately 0.6 % nitrogen, indicative of the presence of a molecule containing a nitrogen atom, namely ODI. Furthermore, the oxygen concentration decreased from 52.23 % to 50.87 %, while carbon content increased from 39.9 % to 48.03 %, suggesting the grafting of a molecule with a notably higher carbon content. The concentration of carbon in the ODI-*g*-starch was subsequently employed to calculate the degree of substitution (DS) of the grafted ODI molecules, as per Eq. (1). The calculated DS value of 0.067 indicated the grafting of approximately 7 ODI molecules per 100 anhydroglucose units.

This DS value was then utilized to determine the weight percent of grafted ODI molecules, considering the molecular weights of the anhydroglucose unit (162.14 g/mol) and ODI (295.5 g/mol). As detailed in Table 2, the weight percent of grafted ODI was found to be 12.27 %, aligning closely with the observations from the TGA results. To the best of the authors' knowledge, no prior reports existed on the surface treatment of starch using ODI molecules. Nevertheless, the concentration of grafted ODI in this study corresponded well with that documented for ODI-grafted cellulose materials [33,60]. Importantly, the grafting of ODI molecules resulted in a transformation of the starch's properties, transitioning it from a hydrophilic material to a hydrophobic one. This transformation could potentially impact the compatibility of starch with polymer matrices, such as PLA. Additionally, Fig. S3 presents the contact angle of a water droplet on the surface of ODI-*g*-starch, along with a photo taken 48 h after dispersing the surface-treated starch in water. These visuals offer insights into the level of hydrophobicity achieved with the surface treatment, further highlighting its effects.

Subsequently, the microstructure of the starch particles was

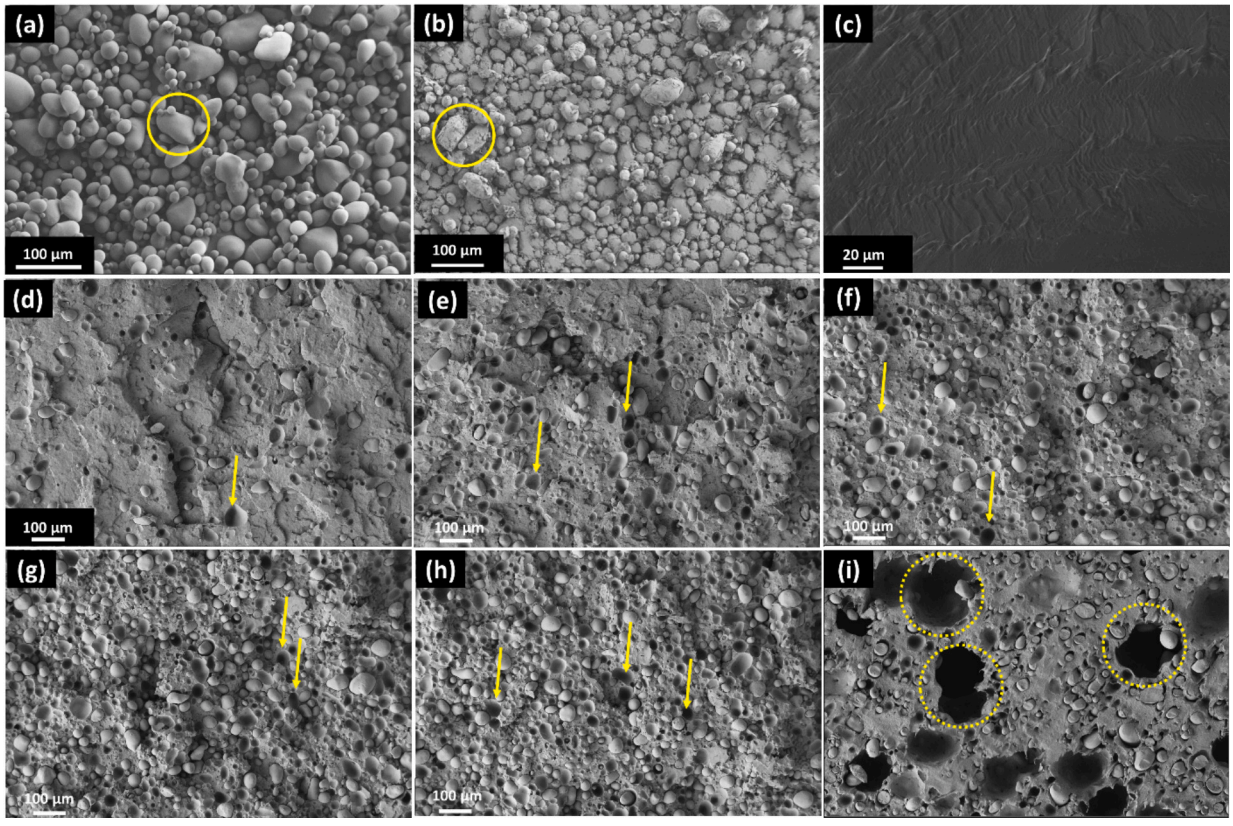

Fig. 3. SEM images of starch a) before and b) after the surface treatment with ODI (magnification of 150×). SEM images from the cryofracture surface area of c) PLA, d) P90S10, e) P80S20, f) P70S30, g) P60S40, h) P50S50, and (i) biocomposite containing 50 % untreated starch.

examined both before and after the surface treatment, utilizing SEM images. As illustrated in Fig. 3a, native potato starch displayed oval and well-defined granular structures with an average particle size of 32 ± 18 μm, a pattern reminiscent of those observed in banana and potato starch studies [55]. Additionally, the surface of these particles appeared smooth and devoid of any discernible defects. Upon undergoing the surface treatment (Fig. 3b), the particles' overall shape remained largely unchanged. However, notable alterations became apparent on the surface of the modified starch, as evidenced by the comparison of the particles highlighted by circles in Fig. 3a and Fig. 3b. These included depressions, ruptures, and numerous furrows, rendering the surface somewhat flaky and porous—a transformation observed consistently in previous studies of surface-modified starch particles [61,62]. It's noteworthy that, in contrast to certain literature sources [63,64], there was no significant reduction in particle size attributable to the hydrolysis effect of modifier molecules, nor were there any indications of spot formation or crack development on the starch granules' surface.

3.2. Microstructure of biocomposites

The morphology of materials plays a pivotal role in determining their properties. Consequently, the microstructure of both plain PLA and biocomposites was scrutinized through SEM imaging, as presented in Fig. 3c to Fig. 3i. In the case of plain PLA (Fig. 3c), the examination revealed a smooth cryofracture cross-section surface devoid of voids, cracks, or particles. This observation suggests that plain PLA is prone to fracture at very low temperatures, as previously reported [65]. In contrast, for the biocomposites, the ODI-*g*-starch particles were uniformly dispersed within the PLA matrix, displaying no indications of particle agglomeration, phase separation, or crack formation. These findings indicate enhanced interfacial adhesion and harmonious compatibility between PLA and starch particles [66].

Furthermore, the size and shape of the particles exhibited minimal alteration. Unlike the study by Yoksan et al. [65], no evidence of droplet-matrix morphology or a co-continuous structure indicative of phase separation was observed. However, it should be noted that in all biocomposites, some starch particles were not entirely encapsulated by the PLA matrix, and instances of particle pulling out were evident, as highlighted by arrows. This suggests that while the employed compatibilization method contributed to improved compatibility between the phases, it may not have achieved complete compatibility. Notably, phase separation and void formation were more pronounced in the biocomposite containing 50 % untreated starch (circles in Fig. 3i), highlighting the incompatibility between components owing to the differing hydrophobic nature of PLA and starch phases [66]. This underscores the beneficial impact of starch surface modification in enhancing compatibility between the phases, ultimately reducing phase separation and void formation.

3.3. Study of crystallinity

The thermal properties of both plain PLA and biocomposites were comprehensively evaluated, encompassing the glass transition temperature (T_g), cold crystallization temperature (T_{cc}), melting temperature (T_m), crystallization temperature (T_c), and the crystallinity (χ_c) of the samples, utilizing DSC thermograms. These thermograms, encompassing the first and second heating cycles, as well as the first cooling cycle, are thoughtfully presented in Fig. 4a to Fig. 4c. Additionally, Table 3 compiles the pertinent data extracted from these curves.

During the initial heating cycle, ODI-*g*-starch exhibited T_g and T_m values of 69 °C and 117 °C, respectively (Fig. 4a), accompanied by a narrow endothermic peak. Conversely, native starch displayed a broad endothermic peak during the same heating cycle without any discernible phase transition (Fig. 4d). The observed T_g in ODI-*g*-starch suggested that the grafting of relatively long aliphatic moieties, i.e., ODI, induced increased molecular chain mobility characterized by an expanded free

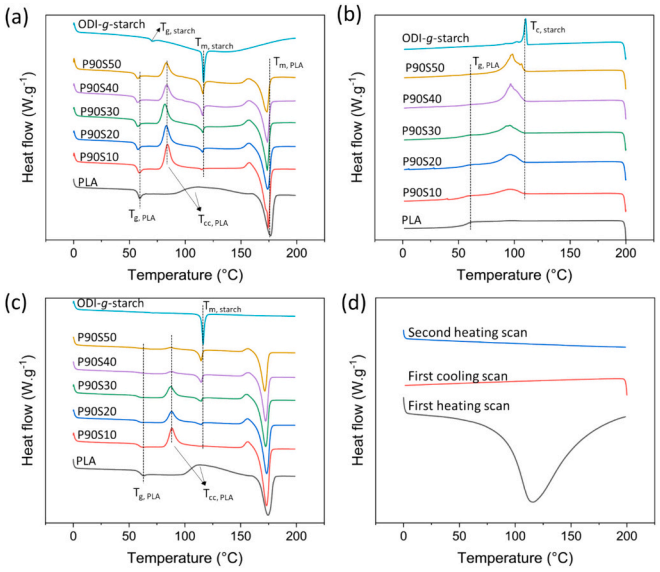

Fig. 4. DSC thermograms of PLA and biocomposites with different concentrations of ODI-*g*-starch. a) first heating scan, b) first cooling scan, and c) second heating scan. d) DSC thermograms of starch.

Table 3
DSC data of the plain PLA, biocomposites, and ODI-*g*-starch.[a]

Sample	T_g (°C)	T_{cc} (°C)	T_m (°C)	ΔH_{cc} (J/g)	ΔH_m (J/g)	χ_c (%)
PLA	57	112	177	31.7	42.5	11.6
P90S10	57	84	175	22.9	46.5	28.2
P80S20	56	83	174	18.7	38.1	25.9
P70S30	55	82	174	18.4	35.9	26.9
P60S40	55	84	174	13.7	28.1	25.6
P50S50	55	83	173	12.5	26.5	30.1
ODI-*g*-starch	67	–	117	–	9.8	–

[a] Extracted from the first heating scan.

volume. This, in turn, disrupted the crystalline structure of starch, leading to a typical glass transition within the amorphous region. This phenomenon resulted in a reduction in starch crystallinity, mirroring findings reported by Lee et al. for polydecalactone-grafted cellulose [67]. Notably, the native starch granules typically exhibit a high crystallinity ranging from 14 % to 45 %, presenting challenges in terms of usability and processing. Therefore, pretreatment is often necessary to enhance the mechanical and rheological properties of starch, achieved by reducing its crystallinity to some extent [68].

On the other hand, plain PLA demonstrated distinct T_g and T_m values, as well as an exothermic peak indicative of cold crystallization, attributed to the formation of a disordered α' crystal phase in PLA [67]. Specifically, PLA exhibited T_g, T_{cc}, and Tm values of 57 °C, 112 °C, and 177 °C, respectively. Upon the incorporation of ODI-*g*-starch into the PLA matrix, these temperature values were still observed, albeit with slight shifts. Notably, T_{cc} exhibited a significant decrease of approximately 30 °C, indicating the nucleating effect of starch particles. This effect facilitated greater mobility of PLA chains, thereby accelerating the formation of crystals [25,65]. Additionally, T_g and T_m exhibited slight reductions with increasing starch concentration, transitioning from 57 °C and 177 °C in pure PLA to 55 °C and 173 °C in P50S50, in accordance with literature findings [65,69,70]. Moreover, the intensity of the cold crystallization peak diminished post-blending, signifying an enhancement in PLA crystallization, as reflected in the crystallinity values provided in Table 3. The crystallinity increased from 11.6 % in plain PLA to 30.1 % in P50S50, suggesting the uniform dispersion of surface-modified starch particles, which acted as nucleating sites for the

crystallization of PLA chains. This, in turn, favored the crystallinity of the matrix [2]. In essence, the grafted aliphatic moieties on the starch particles' surface not only did not hinder crystal formation but also promoted it. Worth noting is the consistency of T_g and Tm values in the PLA/starch blends, signifying the potential compatibility between PLA and starch phases due to the applied compatibilization method, in contrast to the reports in the literature where unchanged T_g and Tm were indicative of PLA and starch incompatibility [65].

In the first cooling scan thermogram, as the temperature decreased, pure PLA did not exhibit crystallization behavior induced by the melt phase and solely displayed a glass transition at 59.1 °C. The absence of an exothermic crystallization peak was attributed to the formation of a mesophase containing disordered aggregations of (10/3) helical chain segments when melt PLA was rapidly quenched [67]. T_g slightly decreased with an increase in the ODI-*g*-starch content, indicative of enhanced mobility in PLA chains resulting from the plasticizing effect of surface-modified starch particles [65].

The second heating scan, conducted with the erasure of the samples' thermal history, allowed for a comparison of thermal data. These results have been summarized in Table S9. In contrast to the initial heating cycle, plain PLA exhibited a slight increase in both T_g and T_{cc}, to 59.9 °C and 113.9 °C, respectively, while T_m slightly decreased to 174.5 °C. Notably, all samples featured a single melting point, contrary to literature trends indicating a double melting peak. Multiple melting behavior typically arises from the formation of small or imperfect crystals during the initial cooling scan. The lower-temperature peak is linked to the melting of less perfect α'-crystals formed during the cooling process, while the higher-temperature melting peak results from the melting of more stable α-crystals, characterized by a more ordered crystal structure than the α'-crystals [2,25,65]. In this study, the presence of a single melting peak in the second heating scan suggests that the employed compatibilization chemistry facilitated the formation of highly ordered crystals in the PLA matrix, specifically α-crystals. To further support this observation, the crystallinity data in Table S9 indicates that plain PLA exhibited behavior akin to an amorphous polymer during the second heating process, with a crystallinity of 1.8 %. In contrast, the biocomposites exhibited significantly higher crystallinity, suggesting that the surface-treated starch particles served as nucleating agents for the crystallization of PLA chains, promoting crystal growth. Notably, ODI-*g*-starch exhibited a melting peak at 116.3 °C even in the second heating scan, contrasting with literature reports of starch's melting peak disappearance in the second heating scan due to the difficulties in starch recrystallization during the initial cooling scan [65].

3.4. Mechanical properties

The mechanical properties of biocomposites are pivotal in determining their suitability for various applications. Consequently, the mechanical characteristics of both plain PLA and the developed biocomposites were assessed through tensile and impact testing. Stress-strain curves, along with a comparison of different mechanical properties—comprising tensile modulus, yield stress, tensile strain (or elongation at break), toughness, and impact strength—have been thoughtfully presented in Fig. 5a, Fig. 5b, and Table S10. In its pristine form, PLA displayed a brittle breaking mechanism devoid of any plastic deformation behavior. Conversely, the incorporation of up to 40 wt% of ODI-*g*-starch into the PLA matrix resulted in biocomposites that exhibited ductile behavior, accompanied by distinct yield stress characteristics. With an increase in the proportion of ODI-*g*-starch, the biocomposites demonstrated a substantial enhancement in tensile strength, impact strength, tensile strain, and toughness. The ANOVA (analysis of variance) was further utilized to assess significant differences among the tested groups. Our results from the ANOVA indicated that the differences observed in the mechanical properties, such as tensile strength, impact strength, tensile strain, and toughness, were statistically significant ($p < 0.05$). This suggests that the variations in the proportions of *ODI-g-starch* had a notable impact on the performance of the biocomposites.

Nevertheless, the tensile modulus did not change significantly. In essence, ODI-*g*-starch functioned as a plasticizing agent, enhancing the stretchability of the PLA matrix. These findings are consistent with previous reports on PLA/plasticized starch blends [64,71].

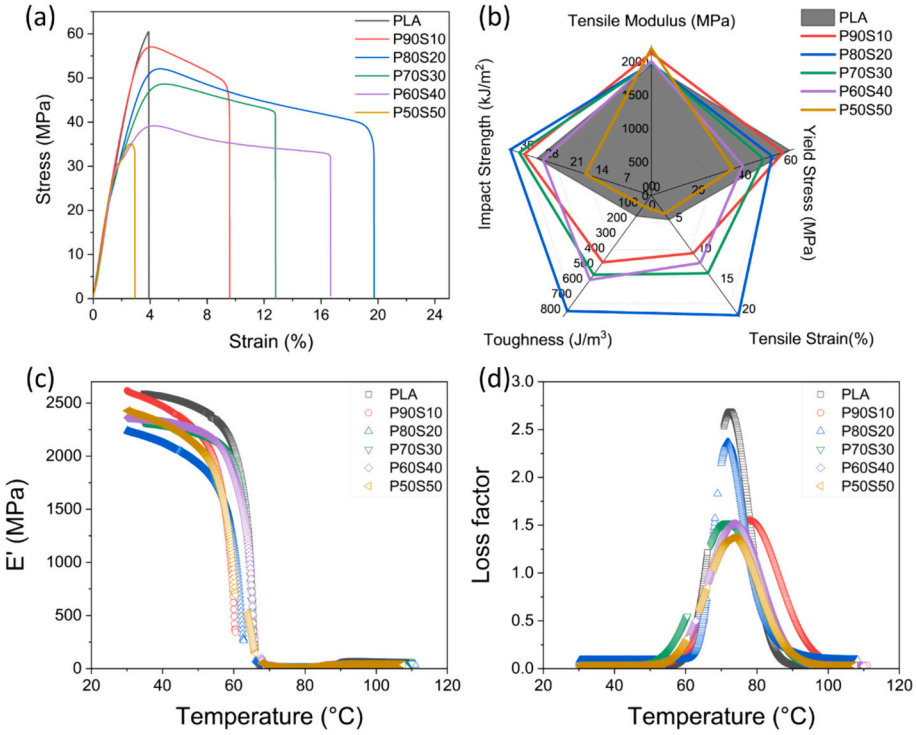

Fig. 5. a) Stress-strain curves, and b) comparison of different mechanical properties. c) Storage modulus (E') and d) loss factor (δ) versus temperature.

The flexibility of the biocomposite containing >40 wt% of ODI-*g*-starch, specifically P50S50, began to diminish. Notably, its tensile strain decreased to 3 %. This suggests that even interfacial modification couldn't significantly improve the rigidity of starch particles at such a high filler content [72]. The compromised mechanical properties of the P50S50 biocomposite could also be attributed to the partial aggregation of starch particles, as observed in the SEM images. Given that both PLA and starch are relatively brittle materials, the grafting of flexible moieties onto the surface of starch may not substantially enhance the blend's stretchability at a high concentration of 50 wt%. This aligns with findings related to the incorporation of thermoplastic cassava starch into PLA [65,73].

3.5. Viscoelastic behavior

The viscoelastic behavior of both plain PLA and the developed biocomposites was thoroughly assessed through DMA and rheology tests. Storage modulus (E') and tan delta (tan δ) as functions of temperature have been illustrated in Fig. 5c and Fig. 5d. For all samples, E' exhibited a significant decrease between 50 °C and 70 °C, signaling a phase transition from a glassy state to a rubbery state, commonly known as the glass transition temperature (T_g). This transition, accompanied by a peak in the tan δ curves, occurred at approximately 55 °C, aligning with the DSC results and being consistent with the reported T_g of PLA in the literature [74]. The incorporation of ODI-*g*-starch led to alterations in the storage modulus values below Tg. Specifically, the modulus decreased with increasing ODI-*g*-starch content up to 30 wt% loadings, after which it exhibited a slight increase. This behavior can be attributed to the flexibility of the ODI-*g*-starch particles, effectively acting as a plasticizing agent, a phenomenon also observed in the tensile testing results. Similar findings have been reported for PLA/thermoplastic starch blends [66]. Importantly, there were no discernible ruptures in the E' curves, indicating a strong interfacial adhesion between ODI-*g*-starch and the PLA matrix. This strong adhesion was a critical factor for the efficient transfer of stress between the two phases [64].

In contrast, T_g did not undergo significant changes with increasing ODI-*g*-starch loading. However, the tan δ values were lower in the biocomposites compared to plain PLA, suggesting that PLA became more elastic (less viscous) after blending. This phenomenon can be explained by the uniform distribution of ODI-*g*-starch particles, which enhanced interactions between the two phases, consequently limiting the mobility of PLA chains during the transition [75].

Rheological properties can yield valuable insights into the interfacial characteristics of polymer components in blends. Consequently, the rheological properties of both plain PLA and the biocomposites were investigated in the molten state using a rotational rheometer with parallel geometries. All measurements were conducted within the viscoelastic region, as determined by a strain sweep test spanning from 0.01 % to 100 % shear strain (Fig. S4). The storage and loss moduli (G' and G"), along with complex melt viscosity versus frequency, are depicted in Fig. 6a and Fig. 6b. In all samples, G" consistently exceeded G' across the entire frequency range, signifying that the samples exhibited greater viscous properties than elastic ones under the test conditions. In essence, the molten samples displayed a liquid-like or terminal behavior rather than a solid-like one, wherein the polymer chains were fully relaxed [76–78]. This relaxation was unimpeded by the starch particles, indicating effective compatibilization [79]. Furthermore, both moduli, G' and G", were higher in pure PLA compared to the biocomposites, suggesting reduced rigidity of the PLA matrix in the presence of plasticized starch domains, a phenomenon also observed by other researchers [72].

On the other hand, as observed in similar studies [80], plain PLA and biocomposites containing <30 wt% of surface-treated starch exhibited a distinct Newtonian Plateau at low frequencies, where viscosity remained constant. At higher frequencies, they exhibited non-Newtonian behavior, with viscosity decreasing as frequency increased—a phenomenon known as shear-thinning behavior. This behavior indicates the viability of extrusion and injection molding as blending techniques for these biocomposites. At all frequencies, the viscosity of plain PLA exceeded that of P90S10, P80S20, and P70S30 biocomposites but was lower than the melt viscosity of P60S40 and P50S50 biocomposites at low frequencies. For instance, the zero-shear rate viscosity of PLA was 527 Pa·s, whereas it was 154 Pa·s and 82 Pa·s in P90S10 and P80S20, respectively. This trend aligns with findings reported for PLA/surface-modified starch blends [81,82], indicating the plasticizing effect of ODI-*g*-starch particles. This effect is achieved through the orientation of surface-modified particles with long aliphatic moieties under the applied shear stress, a phenomenon previously observed in the mechanical properties and DMA results.

The higher melt viscosity of biocomposites with greater concentrations of ODI-*g*-starch can be attributed to the formation of a 3D percolated-type structure (agglomerate structure) between PLA and starch particles. Nevertheless, at higher frequencies, significant shear stresses disrupt the pre-formed 3D structures, leading to reduced blend viscosity. As mentioned earlier, the reduced need for an after-pressure step in the biocomposites, in contrast to plain PLA during injection molding, supports the notion that ODI-*g*-starch particles acted as lubricating agents, reducing the melt viscosity of the PLA matrix.

3.6. Preliminary life cycle assessment

3.6.1. Analysis of the carbon footprint

The incorporation of potato starch as the biofiller into the PLA matrix, with varying potato starch contents from 10 wt% to 50 wt%, resulted in notable reductions of up to 18 % in carbon footprint when compared to pure PLA (Fig. 7a). This reduction is attributed to the inherently lower initial carbon footprint associated with potatoes and

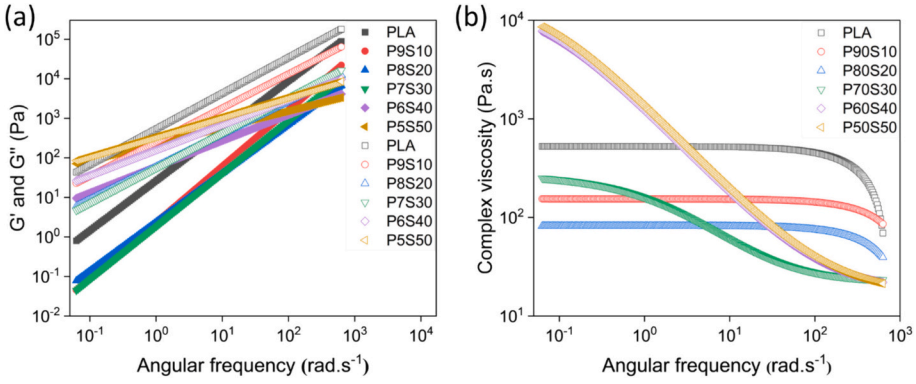

Fig. 6. a) Storage modulus (G', solid symbol) and loss modulus (G", blank symbols) and b) complex viscosity at a fixed shear strain of 10 % and temperature of 210 °C.

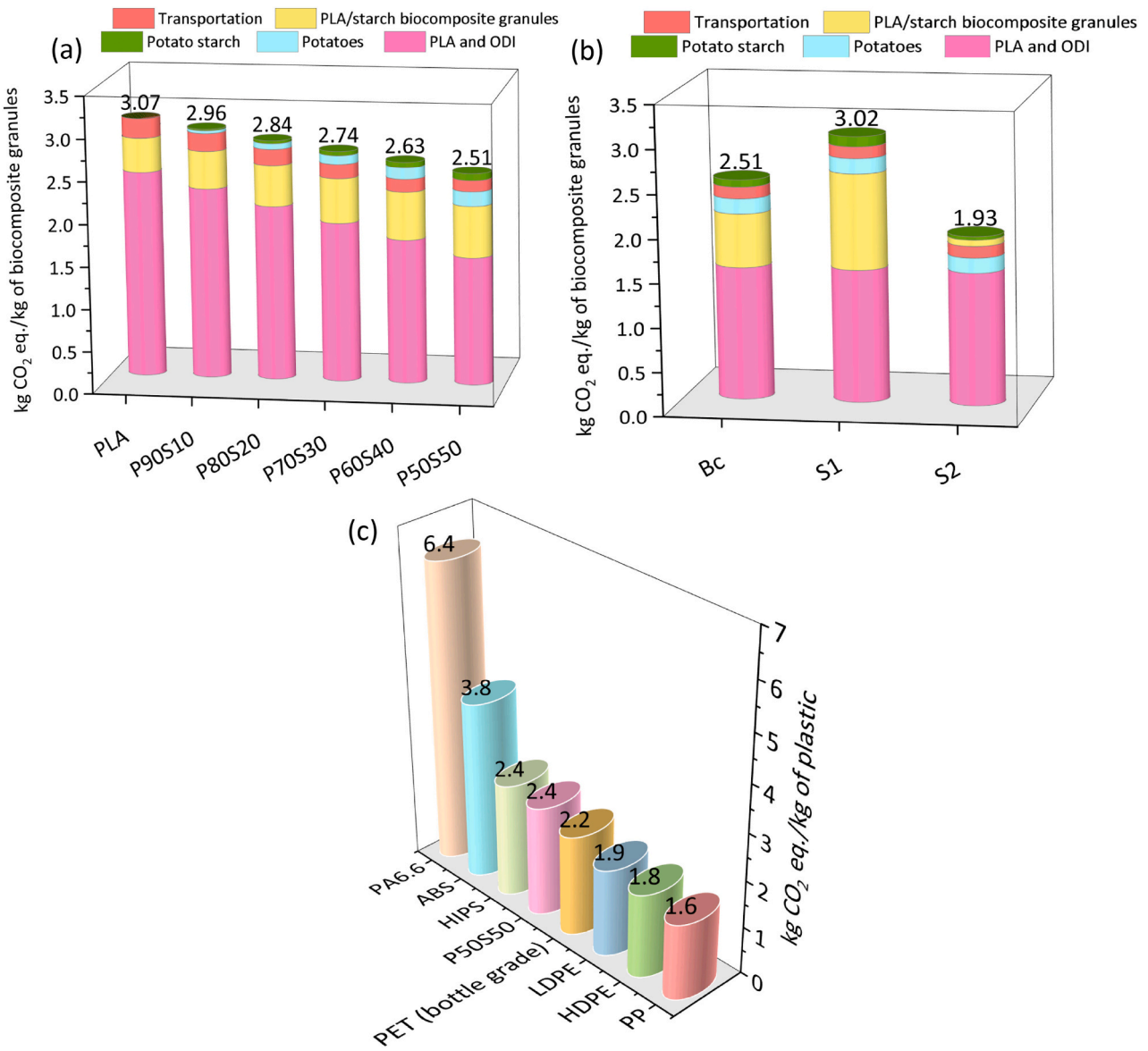

Fig. 7. The carbon footprint of PLA/starch biocomposite granules with varying content of potato starch – the abbreviations of PLA, PA90S10, P80S20, P70S30, P60S40, and P50S50 stand for the plain PLA granules and the biocomposite granules with different percentages of starch (10, 20, 30, 40, and 50 wt%), respectively. a) Baseline case. b) Baseline case (Bc) with sensitivity analysis, including sensitivity analysis scenarios 1 (S1) and 2 (S2), the latter two representing the use of European electricity and global green electricity, respectively. Noteworthy, for the sensitivity analysis graph, the highest potato starch content (50 wt%) was used. Additionally, due to its low amount, sequestered CO_2 in potato starch was not considered in these first two graphs. c) A comparison of PLA/starch biocomposite granules, with the highest potato starch content of 50 wt%, to the selected commercial, fossil-based plastics. For this purpose, the amount of sequestered CO_2 in potato starch has been considered in the carbon footprint of the biocomposite granules.

potato starch, combined with their local production, which involves shorter transportation distances, in contrast to the PLA granules produced in and distributed from the facilities located in Thailand and the Netherlands. This explanation also aligns with the findings presented by Mahalle et al. [40] regarding the carbon footprint of their laboratory-scale PLA/TPS biocomposite.

In more detail, in our analysis, we observed that as the proportion of potato starch added to the PLA matrix increased, certain aspects of the carbon footprint exhibited specific trends. Namely, the carbon footprint associated with potato cultivation increased by 7 %, while the processing and modification of potato starch increased by 3 %, with greater potato starch content in the PLA matrix. Conversely, the carbon footprint related to the production of PLA granules decreased by 19 %, and the transportation of raw materials decreased by 2 %. On another note, the carbon footprint of manufacturing PLA/starch biocomposite granules increased by 11 %, mainly due to the electricity consumption during the laboratory-scale production processes. For most of the impacts arising from the production of PLA/starch biocomposite granules, the production of PLA granules and the ODI played a significant role, accounting for 60 % to 79 % of the total carbon footprint across all the potato starch contents (the carbon footprint of PLA granules and ODI was combined for the analysis, following Sphera Solutions GmbH's guidelines). In general, after the production of PLA granules and ODI, the major contributors to the total carbon footprint were, in the descending order, the production of PLA/starch biocomposite granules at the laboratory scale, transportation of raw materials, potato cultivation, and the processing and modification of potato starch, accounting for 13 % to 24 %, 5 % to 8 %, 0 % to 7 %, and 0 % to 3 % of the total carbon footprint, respectively.

These LCIA results are consistent with the previous LCA studies on

PLA/starch biocomposites with similar functional units and comparable system boundaries [2,83], as also summarized in Table S11. However, slight variations in results may be attributed to factors such as the inclusion of different additives, compatibilizers, industrial-scale production of the biocomposite, as well as considerations for the EoL phase in the studies conducted by these researchers. We also encountered additional studies on PLA/starch biocomposites, but they were not directly comparable to ours due to the differences in functional units [13,40,84], non-comparable system boundaries [13,84], non-standard presentation of the LCIA results [13], or variations in the overall carbon footprint of the biocomposite [40]. However, the phenomenon of a gradual reduction in the carbon footprint of pure PLA with an increasing starch content, as discussed in the existing literature [13], aligned with the findings of the present study. Having said that, it's important to note that the sequestered CO_2 within potato starch, which amounted to 0.16 kg CO_2 eq./kg of biocomposite granules, was factored into the analysis in this subsection. Nevertheless, the LCIA results for the highest potato starch content, which includes the sequestered CO_2, are presented in Table 4.

3.6.2. Results of the applied sensitivity analyses

For the sensitivity analysis, we focused on PLA/starch biocomposite granules containing 50 wt% of potato starch. These granules were chosen because they exhibited the highest electricity consumption within the defined system boundaries, when compared to biocomposites with a lower potato starch content. As illustrated in Fig. 7b, the application of European electricity led to a 17 % increase in the carbon footprint of the biocomposite granules, while the use of a global green electricity reduced it by 23 %, when compared to the baseline scenario. This finding aligns with the expectations and can be attributed to Europe's relatively higher reliance on fossil fuels for electricity generation [85,86], in contrast to the environmentally friendlier nature of green electricity, which produces fewer CO_2 emissions and has a lower global warming potential (GWP), when compared to traditional thermal power generation with fossil fuels [87].

3.6.3. Comparison of the biocomposites to fossil-based plastics

Fig. 7c provides a concise comparison of the carbon footprint of PLA/starch biocomposite granules with the highest potato starch content (50 wt%) to a selection of commercially available, fossil-based plastics. Specifically, the LCI data for low-density polyethylene (LDPE), high-density polyethylene (HDPE), PP, and polyamide 66 (PA66) were sourced from the reports by Plastics Europe [88–90], while the data for acrylonitrile butadiene styrene (ABS), high impact polystyrene (HIPS), and Polyethylene terephthalate (PET) were obtained from the relevant websites and scientific literature, respectively [11,91]. As depicted in Fig. 7c, the carbon footprint of PLA/starch biocomposite granules was reduced by 3 %, 38 %, and 63 %, when compared to fossil-based HIPS, ABS, and PA66, respectively. However, it increased by 9 %, 20 %, 23 %, and 31 % in comparison to fossil-based PET, LDPE, HDPE, and PP, respectively. To enhance the competitiveness of PLA/starch biocomposite granules with these fossil-based reference plastics, certain process adjustments are warranted. These adjustments may involve minimizing the quantity of required compatibilizer, optimizing or consolidating energy-intensive laboratory procedures, shortening reaction times, and adopting entirely green electricity sources. In this context, as explored in the previous subsection, the utilization of global green electricity has the potential to theoretically reduce the carbon footprint of PLA/starch biocomposite granules with 50 wt% of potato starch content to as low as 1.76 kg CO_2 eq./kg of biocomposite granules. This achievement places the carbon footprint slightly below that of both fossil-based LDPE and HDPE used as reference materials.

In addition to the previously mentioned methods for reducing the carbon footprint of PLA/starch biocomposite granules, it is essential to implement changes in the production chain of PLA granules. These changes may involve enhancements in the agricultural practices, the optimization of fertilizer application, increased energy efficiency, a greater reliance on renewable energy sources, and a reduction in the use of chemicals [12]. These improvements, coupled with targeted efforts to shorten the extensive transportation distances associated with the PLA granules, have the potential to significantly reduce the overall carbon footprint of the PLA/starch biocomposite discussed in this study. Furthermore, additional carbon footprint reductions can be achieved by blending the current PLA/starch biocomposite granules with different natural fibers or by combining plain PLA with other bio-based filler alternatives. These alternatives may include materials such as wood pulp, dried distillers grains (DDGS), or rice husks, which are known to have relatively low reported environmental impacts [14]. Pine needles and kenaf fibers also present viable options [15]. It is important to note, however, that there may be trade-offs in the properties of various PLA-based biocomposites when compared to pure PLA. These trade-offs could include a partial degradation of material properties in the biocomposites, although they may also bring potential improvements in environmental impacts and cost reductions, as explored in this study [14]. Similarly, underscored is the need to strike a balance between the environmental considerations and technical performance in composites, as these aspects do not necessarily evolve in lockstep [13]. Therefore, finding a viable compromise is essential.

3.6.4. Recommendations for further enhancement

The sensitivity of electricity consumption to various data and process assumptions became apparent during the course of this LCA study. This underscores the need to establish a more robust methodology for accurately estimating equipment usage times and power requirements in future investigations. Moreover, the utilization of a blend of aliphatic isocyanates as a proxy for ODI may have marginally overestimated its actual environmental impacts due to the inclusion of a greater number of isocyanates in this proxy dataset. To gain a more comprehensive understanding of the environmental impacts associated with the PLA/starch biocomposite granules examined in this study, it is also advisable to expand the scope of the impact categories considered. Additionally, incorporating the EoL stage, encompassing composting, mechanical and chemical recycling, and/or incineration, into future LCA calculations is highly recommended. Lastly, following the necessary process adjustments based on the LCIA results obtained, upscaling the laboratory-scale setup to an industrial scale holds significant potential for further LCA studies and the advancement of these biocomposites.

3.7. 3D printing

Despite the P50S50 biocomposite exhibiting comparatively lower mechanical properties, it was selected as the material for filament production in 3D printing due to its high starch content and the potential eco-friendliness it represents among all the biocomposites developed. To assess the printability of the newly formulated biocomposites, a variety of shapes, including simple cups, dog-bone specimens, 3D curvatures, and intricate grid geometries, were successfully printed using the filament derived from the P50S50 sample. Fig. 8 and Fig. S5 provide CAD models and photographs of the printed pieces, respectively. Notably, the printing process proceeded smoothly under the original feasible fabrication conditions designed for commercial PLA filaments, requiring no

Table 4
The carbon footprint of PLA/starch biocomposite granules with 50 wt% of potato starch for the baseline case as well as the sensitivity analysis scenarios 1 and 2, respectively. The amount of sequestered CO_2 in potato starch has been considered in the values below.

Case type	Carbon footprint	Unit
Baseline case	2.35	kg CO_2 eq./kg of biocomposite granules
Scenario 1	2.86	kg CO_2 eq./kg of biocomposite granules
Scenario 2	1.76	kg CO_2 eq./kg of biocomposite granules

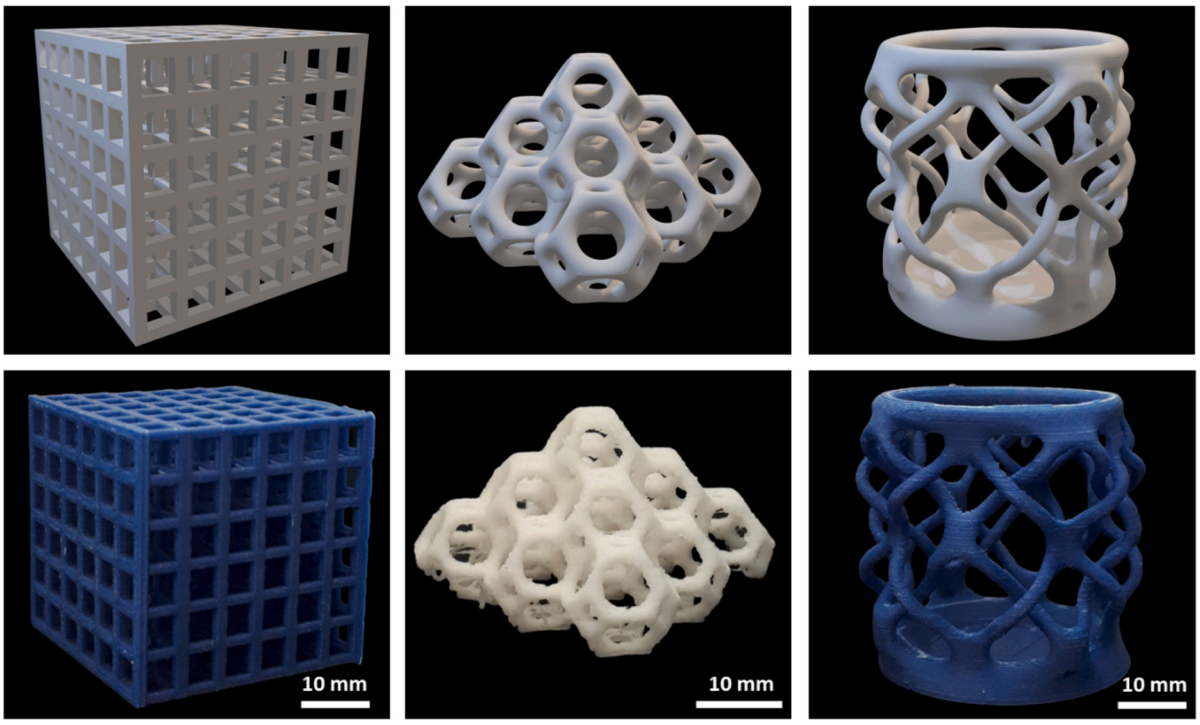

Fig. 8. CAD models (top) and FDM 3D printed objects with the filament developed by the P50S50 biocomposite (bottom). In the blue samples, a little indigo dye was added during the melt blending in the extruder.

additional parameter optimization. Throughout the printing process, there were no issues such as nozzle clogging or filament breakage. Furthermore, there was no delamination between layers and no curling, and the printed objects were easily detached from the build plate, indicating excellent stability of the extruded filaments and strong adhesion between layers [92,93]. Moreover, the printed constructs exhibited minimal fiber debris, presented smooth surfaces, and showed no signs of defects or discontinuities, such as voids, cracks, or excessive roughness. They maintained precise dimensions with no noticeable shrinkage, confirming the success of the printing process [94]. For example, the dimensions of the printed dog-bone specimen closely matched those of the original design (Fig. S6). In summary, the developed filament presents a promising alternative to commercially available PLA filaments, demonstrating its suitability for effective FDM 3D printing.

4. Future and outlook

The study's findings hold significant promise for the future of sustainable materials. The successful grafting of ODI molecules onto starch particles not only enhances the compatibility of starch with the PLA matrix but also opens the door for further improvements in the biocomposite development. This environmentally friendly PLA/starch biocomposite, particularly the variant with 50 wt% of potato starch content, shows potential for reduced carbon footprint compared to petroleum-based plastics. Its ability to create high-quality filaments suitable for 3D printing also suggests a wide range of applications across industries. As sustainability becomes an ever more pressing concern, the adoption of such biodegradable materials is likely to grow, potentially reshaping both the market and regulatory landscape. Collaboration and continued research in this field could further advance the production and application of these innovative materials, contributing to a more eco-friendly future.

5. Conclusions

In the present paper, a series of PLA/starch biocomposites were prepared and characterized. Firstly, the surface of the starch particles was functionalized through a urethane reaction with ODI molecules, resulting in ODI-*g*-starch with enhanced compatibility with the PLA matrix, which can be attributed to the transformation of ODI-*g*-starch from hydrophilic to hydrophobic material. Subsequently, various concentrations of ODI-*g*-starch were melt-blended with the PLA matrix, leading to their homogeneous dispersion within the matrix, which experienced plasticization with an increasing ODI-*g*-starch content. This plasticization effect further led to reductions in the yield stress, complex viscosity, and storage modulus of the biocomposites, with simultaneous enhancements in the elongation at break. Furthermore, ODI-*g*-starch served as a nucleating agent, elevating the crystallinity of the PLA matrix in both the initial and subsequent heating scans, as evidenced in the DSC thermograms.

Along with these, a preliminary LCA was conducted to assess the environmental impacts of the newly developed PLA/starch biocomposite granules in their early stages of development. This analysis revealed notable reductions in the carbon footprint of these biocomposite granules with reductions of up to 18 % when compared to plain PLA granules and 3 %, 38 %, and 63 % in comparison to fossil-based ABS, HIPS, and PA66, respectively. Finally, a uniform filament was successfully fabricated by using the PLA/starch biocomposite with 50 wt% of ODI-*g*-starch, followed by the printing of various geometries with precise dimensions and high surface quality. In conclusion, in the present paper, we introduced novel PLA/starch biocomposites, particularly the variant with the highest potato starch content (50 wt%), as more environmentally friendly alternatives to commercially available, plain PLA granules and specific petroleum-based plastics. These developed biocomposites also possessed improvements in their mechanical properties, crystallinity, and viscoelastic performance, respectively, with great potential for practical applications.

CRediT authorship contribution statement

Hossein Baniasadi: Writing – original draft, Visualization, Supervision, Project administration, Methodology, Investigation, Conceptualization. **Laura Äkräs:** Writing – original draft, Visualization, Methodology, Investigation, Formal analysis, Conceptualization. **Zahra Madani:** Visualization, Formal analysis. **Frans Silvenius:** Investigation, Formal analysis. **Mahyar Fazeli:** Investigation, Formal analysis. **Sami Lipponen:** Visualization, Formal analysis. **Jaana Vapaavuori:** Writing – review & editing, Supervision, Resources, Funding acquisition. **Jukka Seppälä:** Writing – review & editing, Supervision, Resources, Funding acquisition.

Declaration of competing interest

The authors declare that they have no known competing financial interests or personal relationships that could have appeared to influence the work reported in this paper.

Data availability

Data will be made available on request.

Acknowledgment

The authors would like to acknowledge the funding of the Academy of Finland: No. 327248 (ValueBiomat) and No. 327865 (Bioeconomy). Additionally, ZM and JV acknowledge the NordForsk “Beyond e-Textiles” project funding.

Appendix A. Supplementary data

Supplementary data to this article can be found online at https://doi.org/10.1016/j.ijbiomac.2024.135173.

References

[1] J. Muller, C. González-Martínez, A. Chiralt, Combination of poly (lactic) acid and starch for biodegradable food packaging, Materials 10 (2017) 952.
[2] F. Serra-Parareda, M. Delgado-Aguilar, F.X. Espinach, P. Mutjé, S. Boufi, Q. Tarrés, Sustainable plastic composites by polylactic acid-starch blends and bleached kraft hardwood fibers, Compos. B Eng. 238 (2022) 109901.
[3] P. Chotiprayon, B. Chaisawad, R. Yoksan, Thermoplastic cassava starch/poly (lactic acid) blend reinforced with coir fibres, Int. J. Biol. Macromol. 156 (2020) 960–968.
[4] Y. feng Zuo, J. Gu, Z. Qiao, H. Tan, J. Cao, Y. Zhang, Effects of dry method esterification of starch on the degradation characteristics of starch/polylactic acid composites, Int. J. Biol. Macromol. 72 (2015) 391–402.
[5] N.H. Yusoff, K. Pal, T. Narayanan, F.G. de Souza, Recent trends on bioplastics synthesis and characterizations: Polylactic acid (PLA) incorporated with tapioca starch for packaging applications, J. Mol. Struct. 1232 (2021) 129954.
[6] A. Sadeghi, S.M.A. Razavi, D. Shahrampour, Fabrication and characterization of biodegradable active films with modified morphology based on polycaprolactone-polylactic acid-green tea extract, Int. J. Biol. Macromol. 205 (2022) 341–356.
[7] A. Przybytek, M. Sienkiewicz, J. Kucińska-Lipka, H. Janik, Preparation and characterization of biodegradable and compostable PLA/TPS/ESO compositions, Ind. Crop. Prod. 122 (2018) 375–383.
[8] Y. Yan, L. Zhang, X. Zhao, S. Zhai, Q. Wang, C. Li, X. Zhang, Utilization of lignin upon successive fractionation and esterification in polylactic acid (PLA)/lignin biocomposite, Int. J. Biol. Macromol. 203 (2022) 49–57.
[9] Y. Zuo, J. Gu, L. Yang, Z. Qiao, H. Tan, Y. Zhang, Preparation and characterization of dry method esterified starch/polylactic acid composite materials, Int. J. Biol. Macromol. 64 (2014) 174–180.
[10] S. Shaikh, H. Baniasadi, S. Mehrotra, R. Ghosh, P. Singh, J.V. Seppälä, A. Kumar, Strontium-substituted Nanohydroxyapatite-incorporated poly (lactic acid) composites for orthopedic applications: bioactive, machinable, and high-strength properties, Biomacromolecules 24 (2023) 4901–4914.
[11] E.T.H. Vink, S. Davies, Life cycle inventory and impact assessment data for 2014 Ingeo® polylactide production, Ind. Biotechnol. 11 (2015) 167–180.
[12] A. Morão, F. De Bie, Life cycle impact assessment of polylactic acid (PLA) produced from sugarcane in Thailand, J. Polym. Environ. 27 (2019) 2523–2539.
[13] S.A. de Oliveira, J.R.N. de Macedo, D. Dos Santos Rosa, Eco-efficiency of poly (lactic acid)-Starch-Cotton composite with high natural cotton fiber content: environmental and functional value, J. Clean. Prod. 217 (2019) 32–41.
[14] R. Haylock, K.A. Rosentrater, Cradle-to-grave life cycle assessment and techno-economic analysis of polylactic acid composites with traditional and bio-based fillers, J. Polym. Environ. 26 (2018) 1484–1503.
[15] L. Operato, L. Vitiello, P. Aprea, V. Ambrogi, M. Salzano de Luna, G. Filippone, Life cycle assessment of poly(lactic acid)-based green composites filled with pine needles or kenaf fibers, J. Clean. Prod. 387 (2023) 135901.
[16] J.O. Akindoyo, M.D.H. Beg, S. Ghazali, M.R. Islam, Effects of poly (dimethyl siloxane) on the water absorption and natural degradation of poly (lactic acid)/oil-palm empty-fruit-bunch fiber biocomposites, J. Appl. Polym. Sci. 132 (2015).
[17] M. Subbuvel, P. Kavan, Preparation and characterization of polylactic acid/fenugreek essential oil/curcumin composite films for food packaging applications, Int. J. Biol. Macromol. 194 (2022) 470–483.
[18] M. Fazeli, Development of Hydrophobic Thermoplastic Starch Composites, 2018.
[19] J. Yang, Y.C. Ching, C.H. Chuah, D.H. Nguyen, N.-S. Liou, Synthesis and characterization of starch/fiber-based bioplastic composites modified by citric acid-epoxidized palm oil oligomer with reactive blending, Ind. Crop. Prod. 170 (2021) 113797.
[20] M. Fazeli, J. Lipponen, Developing self-assembled starch nanoparticles in starch nanocomposite films, ACS Omega 7 (2022) 44962–44971.
[21] S. Roy Goswami, S. Sudhakaran Nair, S. Wang, N. Yan, Recent Progress on starch maleate/polylactic acid blends for compostable food packaging applications, ACS Sustain. Chem. Eng. 10 (1) (2021) 3–15.
[22] X. Zhou, R. Yang, B. Wang, K. Chen, Development and characterization of bilayer films based on pea starch/polylactic acid and use in the cherry tomatoes packaging, Carbohydr. Polym. 222 (2019) 114912.
[23] S. Mohammadpour Velni, H. Baniasadi, A. Vaziri, Fabrication and characterization of antimicrobial starch-based nanocomposite films and modeling the process parameters via the RSM, Polym. Compos. 39 (2018).
[24] S. Afshar, H. Baniasadi, Investigation the effect of graphene oxide and gelatin/starch weight ratio on the properties of starch/gelatin/GO nanocomposite films: the RSM study, Int. J. Biol. Macromol. 109 (2018).
[25] B. Palai, M. Biswal, S. Mohanty, S.K. Nayak, In situ reactive compatibilization of polylactic acid (PLA) and thermoplastic starch (TPS) blends; synthesis and evaluation of extrusion blown films thereof, Ind. Crop. Prod. 141 (2019) 111748.
[26] R. Ortega-Toro, A. López-Córdoba, F. Avalos-Belmontes, Epoxidised sesame oil as a biobased coupling agent and plasticiser in polylactic acid/thermoplastic yam starch blends, Heliyon 7 (2021) e06176.
[27] D. Briassoulis, A. Pikasi, M. Hiskakis, A. Arias, M.T. Moreira, S.M. Ioannidou, D. Ladakis, A. Koutinas, Life-cycle sustainability assessment for the production of bio-based polymers and their post-consumer materials recirculation through industrial symbiosis, Curr. Opin. Green Sustain. Chem. 41 (2023) 100818.
[28] L. Äkräs, R.M. Ballardini, A. Alén-Savikko, J. Seppälä, Towards sustainable and circular practices with plastics: exploring the potential of law and governance tools based on holistic and harmonized life cycle assessment, Retfærd 2022 (2022) 43–63.
[29] L. Äkräs, M. Vahvaselkä, F. Silvenius, J. Seppälä, H. Ilvesniemi, A multi-criteria decision-making framework and analysis of vegetable oils to produce bio-based plastics, Ind. Crop. Prod. 188 (2022) 115584.
[30] V.-D. Mai, D. Kang, Y. Kim, Y. Jang, J. Min, J. Han, S.-K. Kim, Preparation and environmental analysis of biodegradable polylactic acid and modified cellulose nanofiber composites, J. Ind. Eng. Chem. 130 (2024) 401–411.
[31] M. Torsello, S. Ben-Zichri, L. Pesenti, S.M. Kunnath, C. Samorì, A. Pasteris, G. Bacchelli, N. Prishkolnik, U. Ben-Nun, S. Righi, M.L. Focarete, S. Kolusheva, R. Jelinek, C. Gualandi, P. Galletti, Carbon dot/polylactic acid nanofibrous membranes for solar-mediated oil absorption/separation: performance, environmental sustainability, ecotoxicity and reusability, Heliyon 10 (2024) e25417.
[33] H. Baniasadi, J. Trifol, S. Lipponen, J. Seppälä, Sustainable composites of surface-modified cellulose with low–melting point polyamide, Mater. Today Chem. 22 (2021) 100590.
[34] H. Baniasadi, S. Lipponen, M. Asplund, J. Seppälä, High-concentration lignin biocomposites with low-melting point biopolyamide, Chem. Eng. J. 451 (2023) 138564.
[35] H. Baniasadi, Z. Madani, M. Mohan, M. Vaara, S. Lipponen, J. Vapaavuori, J. V. Seppälä, Heat-induced actuator fibers: starch-containing biopolyamide composites for functional textiles, ACS Appl. Mater. Interfaces 0 (2023).
[36] A. Fonseca-García, B.H. Osorio, R.Y. Aguirre-Loredo, H.L. Calambas, C. Caicedo, Miscibility study of thermoplastic starch/polylactic acid blends: thermal and superficial properties, Carbohydr. Polym. 119744 (2022).
[37] S. Gogolewski, A.J. Pennings, Resorbable materials of poly (l-lactide). II. Fibers spun from solutions of poly (l-lactide) in good solvents, J. Appl. Polym. Sci. 28 (1983) 1045–1061.
[38] Internal Organization for Standardization (ISO), ISO 14040:2006, Environmental Management - Life Cycle Assessment - Principles and Framework, 2006, pp. 1–20.
[39] Internal Organization for Standardization (ISO), ISO 14044:2006, Environmental Management—Life Cycle Assessment—Requirements and Guidelines, 2006, pp. 1–46.
[40] L. Mahalle, A. Alemdar, M. Mihai, N. Legros, A cradle-to-gate life cycle assessment of wood fibre-reinforced polylactic acid (PLA) and polylactic acid/thermoplastic starch (PLA/TPS) biocomposites, Int. J. Life Cycle Assess. 19 (2014) 1305–1315.
[41] Google Maps. https://maps.google.com, 2023 (Accessed 20 February 2023).
[42] Fluent Cargo, Find all Cargo Options and Plan your Next International Shipment in Seconds. https://www.fluentcargo.com, 2023. (Accessed 18 February 2023).
[43] SeaRates, Shipping Distance & Time Calculator. https://www.searates.com/services/distances-time/, 2023. (Accessed 19 February 2023).

[44] European Aliphatic Isocyanates Producer Association (ALIPA), About Alipa. https://www.alipa.org/who-we-are/, 2023 (accessed February 26, 2023).
[45] Corbion, Europe, Middle East & Africa. https://www.corbion.com/en/About-Us/Our-company/Our-global-presence/Europe-Middle-East-and-Africa. (Accessed 5 June 2023).
[46] Port of Helsinki, Cargo at the Port of Helsinki, 2023, pp. 1–11. https://www.esitteemme.fi/portofhelsinki/WebView/ (accessed March 2, 2023).
[47] Posti Group OyJ, Toiminta Postin uudessa Espoon Kilon jakelukeskuksessa on käynnistynyt (Operations at the new Kilo distribution centre in Espoo have started), 2017 (Accessed 26 February 2023), https://www.posti.fi/fi/asiakastuki/tiedotteet/20170313_espoon_kilon_jakelukeskus.
[48] J. Pääkkönen, S. Vuorikoski, K. Pirkanniemi, H. Hyytiä, Paras käytettävissä oleva tekniikka (BAT) Suomen perunatärkkelysteollisuudessa (The best available technology (BAT) in the Finnish potato starch industry). Helsinki, 2004.
[49] Vencorex Chemicals, About Us, Who Are we?. https://www.vencorex.com/about-us/, 2023. (Accessed 5 April 2023).
[50] Sphera, Product Sustainability Solutions Software (Formerly known as GaBi). https://gabi.sphera.com/nw-eu-english/software/gabi-universities/, 2023. (Accessed 5 June 2023).
[51] W. Wang, A. Hu, J. Li, G. Liu, M. Wang, J. Zheng, Comparison of physicochemical properties and digestibility of sweet potato starch after two modifications of microwave alone and microwave-assisted L-malic acid, Int. J. Biol. Macromol. 210 (2022) 614–621.
[52] Y. Hao, Y. Chen, Q. Li, Q. Gao, Synthesis, characterization and hydrophobicity of esterified waxy potato starch nanocrystals, Ind. Crop. Prod. 130 (2019) 111–117.
[53] Y. Li, W. Zhang, J. Zhao, W. Li, B. Wang, Y. Yang, J. Sun, X. Fang, R. Xia, Y. Liu, A route of alkylated carbon black with hydrophobicity, high dispersibility and efficient thermal conductivity, Appl. Surf. Sci. 538 (2021) 147858.
[54] E. Ojogbo, R. Blanchard, T. Mekonnen, Hydrophobic and melt processable starch-laurate esters: synthesis, structure–property correlations, J. Polym. Sci. A Polym. Chem. 56 (2018) 2611–2622.
[55] P.A.M. Morales, Á.M.M. Rodríguez, L.N.M. Pardo, B. Vargas, B.L.L. Osorio, Cassava and banana starch modified with maleic anhydride-poly (ethylene glycol) methyl ether (Ma-mPEG): a comparative study of their physicochemical properties as coatings, Int. J. Biol. Macromol. 205 (2022) 1–14.
[56] K.Z. Hafila, R. Jumaidin, R.A. Ilyas, M.Z. Selamat, F.A.M. Yusof, Effect of palm wax on the mechanical, thermal, and moisture absorption properties of thermoplastic cassava starch composites, Int. J. Biol. Macromol. 194 (2022) 851–860.
[57] R. Roostazadeh, T. Behzad, K. Karimi, Isolation and Characterization of Lignin-rich Particles as Byproducts of Bioethanol Production From Wheat Straw to Reinforce Starch Composite Films, 2022.
[58] P. Wongphan, T. Panrong, N. Harnkarnsujarit, Effect of different modified starches on physical, morphological, thermomechanical, barrier and biodegradation properties of cassava starch and polybutylene adipate terephthalate blend film, Food Packag. Shelf Life 32 (2022) 100844.
[59] L. Chen, D. Zhang, L.-F. Wei, W.-J. Zhu, X.-Q. Yan, R. Zhou, Z. Din, W.-P. Ding, T.-Z. Ma, J. Cai, Structural and mechanistic insights into starch microgel/anthocyanin complex assembly and controlled release performance, Int. J. Biol. Macromol. 213 (2022) 718–727.
[60] G. Siqueira, J. Bras, A. Dufresne, New process of chemical grafting of cellulose nanoparticles with a long chain isocyanate, Langmuir 26 (2010) 402–411.
[61] M.D. Teli, A. Mallick, Application of sorghum starch for preparing superabsorbent, J. Polym. Environ. 26 (2018) 1581–1591.
[62] M. Shi, Y. Jing, L. Yang, X. Huang, H. Wang, Y. Yan, Y. Liu, Structure and physicochemical properties of malate starches from corn, potato, and wrinkled pea starches, Polymers (Basel) 11 (2019) 1523.
[63] M. Majzoobi, P. Beparva, A. Farahnaky, F. Badii, Effects of malic acid and citric acid on the functional properties of native and cross-linked wheat starches, Starch-Stärke 66 (2014) 491–495.
[64] H.S. Ghari, H. Nazockdast, Morphology development and mechanical properties of PLA/differently plasticized starch (TPS) binary blends in comparison with PLA/dynamically crosslinked "TPS+ EVA" ternary blends, Polymer (Guildf) 124729 (2022).
[65] R. Yoksan, A. Boontanimitr, N. Klompong, T. Phothongsurakun, Poly (lactic acid)/thermoplastic cassava starch blends filled with duckweed biomass, Int. J. Biol. Macromol. 203 (2022) 369–378.
[66] M. Akrami, I. Ghasemi, H. Azizi, M. Karrabi, M. Seyedabadi, A new approach in compatibilization of the poly (lactic acid)/thermoplastic starch (PLA/TPS) blends, Carbohydr. Polym. 144 (2016) 254–262.
[67] W. Lee, J. Lee, J.W. Chung, S.-Y. Kwak, Enhancement of tensile toughness of poly (lactic acid) (PLA) through blending of a polydecalactone-grafted cellulose copolymer: the effect of mesophase transition on mechanical properties, Int. J. Biol. Macromol. 193 (2021) 1103–1113.
[68] K. Dome, E. Podgorbunskikh, A. Bychkov, O. Lomovsky, Changes in the crystallinity degree of starch having different types of crystal structure after mechanical pretreatment, Polymers (Basel) 12 (2020) 641.
[69] Y. Whulanza, A. Azadi, S. Supriadi, S.F. Rahman, M. Chalid, M. Irsyad, M. H. Nadhif, P. Kreshanti, Tailoring mechanical properties and degradation rate of maxillofacial implant based on sago starch/polylactid acid blend, Heliyon 8 (2022) e08600.
[70] M.F. Mina, M.D.H. Beg, M.R. Islam, A. Nizam, A. Alam, R.M. Yunus, Structures and properties of injection-molded biodegradable poly (lactic acid) nanocomposites prepared with untreated and treated multiwalled carbon nanotubes, Polym. Eng. Sci. 54 (2014) 317–326.
[71] S. Collazo-Bigliardi, R. Ortega-Toro, A. Chiralt, Using grafted poly (ε-caprolactone) for the compatibilization of thermoplastic starch-polylactic acid blends, React. Funct. Polym. 142 (2019) 25–35.
[72] M. Esmaeili, G. Pircheraghi, R. Bagheri, V. Altstädt, Poly (lactic acid)/coplasticized thermoplastic starch blend: effect of plasticizer migration on rheological and mechanical properties, Polym. Adv. Technol. 30 (2019) 839–851.
[73] H. Hu, A. Xu, D. Zhang, W. Zhou, S. Peng, X. Zhao, High-toughness poly (lactic acid)/starch blends prepared through reactive blending plasticization and compatibilization, Molecules 25 (2020) 5951.
[74] B. Chihaoui, Q. Tarrés, M. Delgado-Aguilar, P. Mutjé, S. Boufi, Lignin-containing cellulose fibrils as reinforcement of plasticized PLA biocomposites produced by melt processing using PEG as a carrier, Ind. Crop. Prod. 175 (2022) 114287.
[75] N. Noivoil, R. Yoksan, Oligo (lactic acid)-grafted starch: a compatibilizer for poly (lactic acid)/thermoplastic starch blend, Int. J. Biol. Macromol. 160 (2020) 506–517.
[76] H. Baniasadi, J. Seppälä, Novel long-chain aliphatic polyamide/surface-modified silicon dioxide nanocomposites: in-situ polymerization and properties, Mater. Today Chem. 20 (2021).
[77] H. Baniasadi, J. Trifol, A. Ranta, J. Seppälä, Exfoliated clay nanocomposites of renewable long-chain aliphatic polyamide through in-situ polymerization, Compos. B Eng. 211 (2021).
[78] H. Baniasadi, S. Borandeh, J. Seppälä, High-performance and biobased polyamide/functionalized graphene oxide nanocomposites through in situ polymerization for engineering applications, Macromol. Mater. Eng. (2021) 2100255.
[79] S. Gu, J. Ren, B. Dong, Melt rheology of polylactide/montmorillonite nanocomposites, J. Polym. Sci. B Polym. Phys. 45 (2007) 3189–3196.
[80] M.A. Aiman, N.A. Ramlee, M.A.M. Azmi, T.N.A.T. Sabri, Preparation, thermal degradation, and rheology studies for polylactic acid (PLA) and palm stearin (PS) blend: a review, Mater. Today Proc. 63 (2022) S222–S230.
[81] Z. Xiong, L. Zhang, S. Ma, Y. Yang, C. Zhang, Z. Tang, J. Zhu, Effect of castor oil enrichment layer produced by reaction on the properties of PLA/HDI-g-starch blends, Carbohydr. Polym. 94 (2013) 235–243.
[82] H. Li, M.A. Huneault, Effect of chain extension on the properties of PLA/TPS blends, J. Appl. Polym. Sci. 122 (2011) 134–141.
[83] M.L.M. Broeren, L. Kuling, E. Worrell, L. Shen, Environmental impact assessment of six starch plastics focusing on wastewater-derived starch and additives, Resour. Conserv. Recycl. 127 (2017) 246–255.
[84] U. Suwanmanee, V. Varabuntoonvit, P. Chaiwutthinan, M. Tajan, T. Mungcharoen, T. Leejarkpai, Life cycle assessment of single use thermoform boxes made from polystyrene (PS), polylactic acid, (PLA), and PLA/starch: cradle to consumer gate, Int. J. Life Cycle Assess. 18 (2013) 401–417.
[85] European Environment Agency, Greenhouse gas emission intensity of electricity generation in Europe. https://www.eea.europa.eu/ims/greenhouse-gas-emission-intensity-of-1, 2023. (Accessed 3 September 2023).
[86] P. Yadav, N. Ismail, M. Essalhi, M. Tysklind, D. Athanassiadis, N. Tavajohi, Assessment of the environmental impact of polymeric membrane production, J. Membr. Sci. 622 (2021) 118987.
[87] C. Gao, S. Zhu, N. An, H. Na, H. You, C. Gao, Comprehensive comparison of multiple renewable power generation methods: a combination analysis of life cycle assessment and ecological footprint, Renew. Sust. Energ. Rev. 147 (2021) 111255.
[88] PlasticsEurope, Eco-profiles and Environmental Product Declarations of the European Plastics Manufacturers: High-density Polyethylene (HDPE), Low-density Polyethylene (LDPE), Linear Low-density Polyethylene (LLDPE), Brussels, Belgium, 2014.
[89] PlasticsEurope, Eco-profiles and Environmental Product Declarations of the European Plastics Manufacturers: Polypropylene (PP), Brussels, Belgium, 2014.
[90] PlasticsEurope, Eco-profiles and Environmental Product Declarations of the European Plastics Manufacturers: Polyamide 6.6 (PA6.6), Brussels, Belgium, 2014.
[91] NatureWorks, Eco-Profile. https://www.natureworksllc.com/sustainability/eco-profile-and-life-cycle-analyses/eco-profile, 2023 (accessed June 19, 2023).
[92] T.B. Freeman, M.A. Messenger, C.J. Troxler, K. Nawaz, R.M. Rodriguez, S.K. S. Boetcher, Fused filament fabrication of novel phase-change material functional composites, Addit. Manuf. 39 (2021) 101839.
[93] H. Baniasadi, D. Chatzikosmidou, J. Seppälä, Innovative integration of pyrolyzed biomass into polyamide 11: sustainable advancements through in situ polymerization for enhanced mechanical, thermal, and additive manufacturing properties, Addit. Manuf. 78 (2023) 103869.
[94] C.-Y. Lee, C.-Y. Liu, The influence of forced-air cooling on a 3D printed PLA part manufactured by fused filament fabrication, Addit. Manuf. 25 (2019) 196–203.
[95] L. Äkräs, et al., A cradle-to-gate life cycle assessment of polyamide-starch biocomposites: carbon footprint as an indicator of sustainability, Clean Technol. Environ. Policy (2024) 1–16.